Structural, electronic, and hyperfine properties of pure and Ta-doped *m*-ZrO_2

M. A. Taylor,[1] R. E. Alonso,[1,2] L. A. Errico,[1,3,*] A. López-García,[1] P. de la Presa,[4] A. Svane,[5] and N. E. Christensen[5]

[1]*Departamento de Física, Instituto de Física La Plata (IFLP, CCT-La Plata, CONICET-UNLP), Facultad de Ciencias Exactas, Universidad Nacional de La Plata, Casilla de Correo 67, 1900 La Plata, Argentina*

[2]*Departamento de Ciencias Básicas, Facultad de Ingeniería, Universidad Nacional de La Plata Calle 47 y 115 S/N La Plata, Argentina*

[3]*Universidad Nacional del Noroeste de la Pcia. de Buenos Aires (UNNOBA), Monteagudo 2772, Pergamino, CP 2700, Buenos Aires, Argentina*

[4]*Instituto de Magnetismo Aplicado, UCM-ADIF-CSIC, P.O. Box 155, 28230 Las Rozas, Spain*

[5]*Department of Physics and Astronomy, Aarhus University, DK-8000 Aarhus C, Denmark*

(Received 8 November 2011; revised manuscript received 20 January 2012; published 6 April 2012)

A combination of experiments and *ab initio* quantum-mechanical calculations has been applied to examine electronic, structural, and hyperfine interactions in pure and Ta-doped zirconium dioxide in its monoclinic phase (*m*-ZrO_2). From the theoretical point of view, the full-potential linear augmented plane wave plus local orbital (APW + lo) method was applied to treat the electronic structure of the doped system including the atomic relaxations introduced by the impurities in the host in a fully self-consistent way using a supercell approach. Different charge states of the Ta impurity were considered in the study and its effects on the electronic, structural, and hyperfine properties are discussed. Our results suggest that two different charge states coexist in Ta-doped *m*-ZrO_2. Further, *ab initio* calculations predict that depending on the impurity charge state, a sizeable magnetic moment can be induced at the Ta-probe site. This prediction is confirmed by a new analysis of experimental data.

DOI: 10.1103/PhysRevB.85.155202 PACS number(s): 71.15.Mb, 76.80.+y, 71.20.Nr

I. INTRODUCTION

Zirconium dioxide (*zirconia*) is one of the most important compounds in materials science and technology because it combines excellent mechanical, thermal, chemical, and dielectric properties:[1–4] high melting point (2700 °C), low thermal and electronic conductivity, good oxygen-ion conductivity at elevated temperatures, high strength and enhanced fracture toughness, chemical inertness, and resistance to corrosion, high dielectric constant, etc. Additionally, ZrO_2 shows a rich variety of crystal structures depending on pressure, temperature, impurity or doping content, growth conditions, etc. In its various forms and (sometimes) with the addition of small amounts of impurities, ZrO_2 has applications, for example, in refractory materials, solid oxide fuel cell electrolytes, catalyst substrates, protective coatings, functional ceramics, ceramic glazes, oxygen sensors, electro-ceramics, and abrasives and grinding media, etc.[5–11] Moreover, zirconia is one of the most radiation-resistant ceramics currently known;[12–14] therefore it has a particular importance in the nuclear industry. Also it was proposed, together with HfO_2, as a gate dielectric material in metal-oxide semiconductor devices.[9,11] For all these basic and technological reasons, the structural and electronic properties of zirconia have been extensively studied by different experimental and theoretical techniques in recent years (see, for example, Ref. 15 and references therein).

Magnetic effects in oxides have gained considerable attention in recent years due to their promising applications in spintronic devices. In addition to its potential utility, the study of spin-polarized transport is revealing new fundamental physics.[16–21] In particular, Coey *et al*. reported ferromagnetism above room temperature in undoped HfO_2 thin films fabricated by conventional out-of-equilibrium pulsed-laser deposition.[22,23] Such unexpected ferromagnetism has also been reported in CaO, ZnO, CaB_6, and ZrO_2 thin films and nanoparticles.[24–27] From a theoretical point of view, it has been shown that point defects such as cation or oxygen vacancies or electron trapping at an impurity site can be the origin of the magnetism.[28–31] Very recently, a combination of hyperfine experiments [using time-differential perturbed angular correlations spectroscopy (TDPAC) with ^{181}Ta as a probe] and *ab initio* calculations has been applied to study the electronic structure of Ta-doped hafnium dioxide.[32] The study revealed that Ta introduces impurity levels in the band gap of semiconducting monoclinic HfO_2 (*m*-HfO_2), and induces significant structural distortions in the host lattice. Also, the structural relaxations as well as the hyperfine parameters strongly depend on the charge state of the impurity. Moreover, the combination of experiments and theory suggests that two different charge states coexist in this compound, and depending on the impurity charge state a sizeable magnetic moment can be induced at the probe site. These results indicate that the trapping of an electron at a cationic site can induce a magnetic moment localized at this site. This trapping effect could be related to the magnetism observed in thin films of pure *m*-HfO_2.[32]

ZrO_2 and HfO_2 are similar systems regarding their chemical and physical properties. They have the same crystallographic structures with very similar cell parameters and atomic positions, and both can be stabilized in their more symmetric structures by means of the addition of low percentages of dopants. Both compounds were studied with TDPAC using ^{181}Ta as a probe (see, for example, Refs. 33,34, and references therein). In consequence, the extension of the combined experimental and theoretical studies to *m*-ZrO_2 is of great interest.

In this work, we present an *ab initio* study in pure and Ta-doped *m*-ZrO_2 including spin-polarized calculations for different charge states. Force calculations were applied to optimize the doped structures relaxing all the atomic positions in the supercell (SC) approximation. From the self-consistent potentials, hyperfine parameters at the Ta site were derived. The influence of the impurity charge state on the hyperfine

parameters and the magnetic state is analyzed. Our results are compared to different experimental and theoretical results reported in the literature and a new analysis of a previous TDPAC experiment is performed.

II. THE SYSTEM UNDER STUDY

Zirconium dioxide is the only thermodynamically stable compound in the system Zr-O.[5,35,36] At low pressures, zirconia displays three phases: monoclinic, tetragonal, and cubic. The ground-state phase of zirconia, a baddeleyite structure with a monoclinic unit cell, is stable up to around 1480 K. The monoclinic unit cell has nine internal degrees of freedom, and contains four ZrO_2 units [m-ZrO_2, space group $P21/c$, Fig. 1(a)]. The four Zr and eight O atoms are located at general positions of C_{2h}^5 ($P2_1/c$): (4c) $\pm(x, y, z)$ and $\pm(-x, y + 1/2, 1/2 - z)$. The x, y, and z values are given in Table I. The unit cell has dimensions $a = 5.1505_1$ Å, $b = 5.2116_1$ Å, $c = 5.3173_1$ Å, and $\beta = 99.230_1$.[37] In this arrangement the Zr atoms exhibit a sevenfold coordination with Zr-O bond lengths between 2.03 and 2.26 Å. There are two kinds of oxygen atoms, which have different coordination: oxygen type 1 (O1) having three Zr neighbors between 2.03 and 2.17 Å, and type 2 (O2) having four Zr neighbors between 2.16 and 2.26 Å (See Fig. 1). The shortest O-O distance is 2.57 Å.

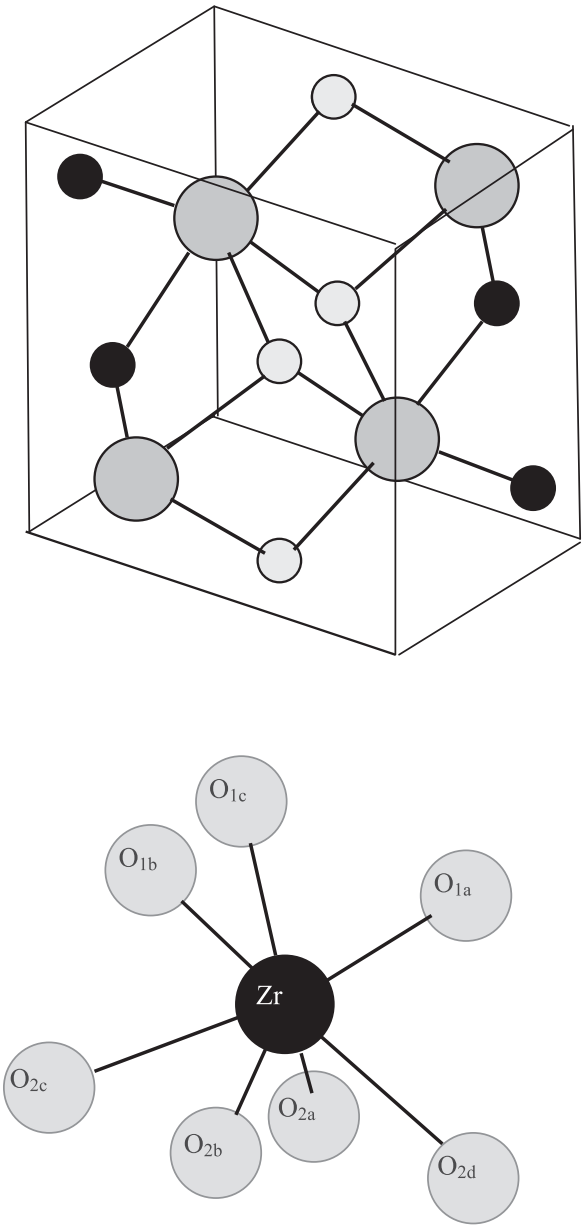

FIG. 1. (a) Monoclinic lattice structure of $m-ZrO_2$. Large spheres represent Zr atoms and small ones O atoms. Black and gray colors distinguish the two nonequivalent O atoms (type 1 and 2) of the structure. (b) The configuration of O atoms in the ZrO_7 polyhedra in m-ZrO_2. Three of seven O atoms are threefold coordinated (atoms type 1) and four of them are fourfold coordinated (atoms type 2).

TABLE I. Calculated and experimentally determined structural parameters for monoclinic ZrO_2 and distances (in Å) from Zr to its O nearest neighbors. Lattice parameters a, b, and c are in Å and β is in degrees. For the calculation of the internal parameters x, y, and z, lattice parameters and angles were fixed at the experimental ones. Experimental data (right column) were taken from Ref. 37.

	LDA	GGA	PBE-sol	Expt.
a	–	–	–	5.1505_1
b	–	–	–	5.2116_1
c	–	–	–	5.3173_1
β	–	–	–	99.230_1
x(Zr)	0.2768	0.2771	0.2769	0.2754
y(Zr)	0.0421	0.0420	0.0425	0.0395
z(Zr)	0.2088	0.2096	0.2094	0.2083
x(O1)	0.0693	0.0690	0.0690	0.0700
y(O1)	0.3331	0.3330	0.3334	0.3317
z(O1)	0.3462	0.3443	0.3450	0.3447
x(O2)	0.4508	0.4484	0.4493	0.4496
y(O2)	0.7573	0.7537	0.7572	0.7569
z(O3)	0.4794	0.4797	0.4795	0.4792
d(Zr-O_{1a})	2.053	2.049	2.050	2.035
d(Zr-O_{1b})	2.068	2.068	2.068	2.058
d(Zr-O_{1c})	2.150	2.151	2.155	2.159
d(Zr-O_{2a})	2.157	2.163	2.157	2.169
d(Zr-O_{2b})	2.162	2.173	2.167	2.193
d(Zr-O_{2c})	2.250	2.246	2.250	2.227
d(Zr-O_{2d})	2.251	2.252	2.251	2.264
d^{mean}	2.155	2.155	2.157	2.158
d^{mean} (EXAFS experiment, Ref. 54)				2.16

III. HYPERFINE PARAMETERS

Nuclear techniques, such as TDPAC or nuclear magnetic resonance (NMR), among others, have been extensively applied to the study of materials in order to elucidate the (sub-) nanoscopic scale environment(s) of impurities or constituent atoms of solids (see Ref. 38 and references therein). What is most rewarding in these methods is their "ability" to measure charge symmetry-related properties, such as the electric field gradients (EFG), as well as magnetic properties, such as magnetic hyperfine fields (B_{HF}), making it possible to obtain a fingerprint of the electronic and magnetic configuration near and at the probe nucleus.[39]

The information provided by these techniques is given as a product of a nuclear and an external nuclear quantity.[39] In the case of pure electric quadrupole interactions, the nuclear quantity is the nuclear quadrupole moment Q, characteristic of a given nuclear state of spin I, which interacts with the EFG at the nuclear position. The EFG tensor is a rank 2 traceless symmetric tensor whose components, denoted by V_{ij}, are defined by the second derivative (with respect to the spatial coordinates) of the Coulomb potential $V(\boldsymbol{r})$ created by the charge density surrounding a given nucleus.[39] In the principal axis system the three diagonal components of the EFG tensor are labeled according to the conventional choice $|V_{XX}| \leqslant |V_{YY}| \leqslant |V_{ZZ}|$. Hence, V_{ZZ} is the largest eigenvalue of the EFG tensor. The measured magnitude is the nuclear coupling constant frequency ν_Q, related to V_{ZZ} by[39]

$$\nu_Q = \frac{eQ\,V_{ZZ}}{h}. \tag{1}$$

The EFG tensor is completely specified by V_{ZZ}, together with the asymmetry parameter η:

$$\eta = \frac{V_{XX} - V_{YY}}{V_{ZZ}}, \tag{2}$$

where $Q = 2.36(5)$ b for the spin 5/2 482 keV excited state of ^{181}Ta (TDPAC-sensitive state, Ref. 40), while $Q = -0.176(3)$ b is the nuclear quadrupole moment of the spin 5/2 ground state of ^{91}Zr (sensitive state in NMR spectroscopy, Ref. 41).

The magnetic hyperfine interaction is caused by the coupling between the magnetic field produced by the electron spin and the orbital currents at the probe site and the magnetic moment of the nucleus. The experimentally observed quantity is, in this case, the precession frequency:[39]

$$\omega_L = \frac{g_N \mu_N B_{HF}}{h}, \tag{3}$$

where g_N denotes the nuclear g factor and μ_N is the nuclear magneton.[42] B_{HF} is the magnetic hyperfine field, which is a fingerprint of the magnetic configuration and the spin polarization near and at the probe nucleus.[39]

Whereas pure quadrupolar and/or pure magnetic interactions have been extensively observed using TDPAC, cases of combined electric and magnetic interaction (CEMI) in which the quadrupolar electric and the dipolar magnetic interactions are of the same order of magnitude are scarce in the literature.[43,44] In the case of a CEMI, the experimentally observed parameters are ν_Q, the asymmetry parameter η, the magnetic frequency ω_L, and the Euler angles β, γ, which describe the relative orientation of the magnetic hyperfine field and the EFG tensor.

IV. CALCULATION DETAILS

We performed *ab initio* electronic structure calculations to determine the self-consistent potential and the charge density inside the m-ZrO_2 cell. From these first-principles calculations the hyperfine parameters at a Ta impurity replacing Zr were obtained, taking properly into account the structural and electronic effects introduced by the impurity in the host lattice. We simulated this nonperiodic system by considering a periodically repeated large unit cell where a single Ta atom replaces a single Zr in the monoclinic ZrO_2 host (the SC method). From these *ab initio* calculations we obtained the equilibrium relaxed structures and the EFG tensor corresponding to a Ta atom at the cation site in the ZrO_2 lattice. The calculations were made for a periodic arrangement of 96-atom SCs, each constructed from eight unit cells of m-ZrO_2. The resulting 96-atom SC has dimensions $a' = 2a = 10.3010$ Å, $b' = 2b = 10.4062$ Å, and $c' = 2c = 10.6308$ Å. The replacing of a single Zr atom in the SC by one Ta atom lead to an ordered compound, $Zr_{0.969}Ta_{0.031}O_2$, representing about 3 at. % doping. Similar to the case of Ta in m-HfO_2, additional calculations were performed (for some selected cases) using larger SCs. These additional calculations show that although a 3 at. % doping is large compared to parts per million (ppm) dilutions in the samples used in the TDPAC experiments, the choice of the 96-atom SC keeps the Ta atoms sufficiently far from each other (10.3 Å) to avoid significant interactions. Thus, the 96-atom SC is an excellent compromise between computational times and accuracy of the calculations.

To solve the scalar-relativistic Kohn-Sham equations, calculations based on the density-functional theory (DFT) (Ref. 45) have been performed with the *ab initio* full-potential augmented plane waves plus local orbitals (APW + lo) method[46] as embodied in the WIEN2K code.[47] Exchange and correlation effects were treated using the local spin density approximation (LSDA),[48] the generalized-gradient approximation [(GGA), Ref. 49], and the Perdew-Burke-Ernzerhof parametrization of GGA for solids (PBE-sol) GGA.[50]

In the APW + lo method the wave functions are expanded in spherical harmonics inside nonoverlapping atomic spheres of radius R_{MT} and in plane waves in the remaining space of the unit cell (the interstitial region). The atomic sphere radii used for Zr, Ta, and O were 1.06, 1.06, and 0.90 Å, respectively. The parameter $RK_{\max}$, which controls the size of the basis set, was set to 6 (R is the smallest muffin-tin radius and $K_{\max}$ the largest wave number of the basis set) for the larger SCs and 8 in the case of the calculations performed in the undoped system. As stated in Ref. 4, zirconium is characterized by a strong overlap of the $4s$, $4p$, and $4d$ wave functions. For this reason we treat the Zr-$4s$, $4p$, $4d$, and $5s$ as valence electrons. To improve linearization, local orbitals[47] were used to describe Zr-$4p$ and $5s$, Ta-$6s$, $5p$, and $4f$, and O-$2s$. Integration in reciprocal space was performed using the tetrahedron method taking up 50 k points in the full Brillouin zone (BZ), which are reduced to 14 k points in the irreducible wedge of the BZ (IWBZ). To plot the density of states (DOS), we calculated eigenvalues at a denser mesh.

In order to get the equilibrium structures, once self-consistency was achieved, quantum-mechanically-derived forces on the ions were obtained, then the ions were displaced according to a Newton-damped scheme, and the relaxed positions of the atoms were obtained (for details see Ref. 51 and references therein). This procedure was repeated until the forces on the ions were below a tolerance value of 0.01 eV/Å. Details of the calculation of the EFG within this code are described in the works of Schwarz *et al.*[52]

To check the accuracy of the present results we performed several additional calculations. For selected systems, we varied the basis set from $RK_{\max} = 5.0$ to $RK_{\max} = 7.0$, and the

number of k points from 50 to 200. Also we examined the effects of changing the muffin-tin radii on the properties of the system. Magnetic moments, electric field gradients, and interatomic distances can be obtained with adequate precision using $RK_{\max} = 6.0$ and 50 k points (the interatomic distances, EFG components, and magnetic moments are converged to error bars smaller than 0.01 Å, 0.5×10^{21} V/m^2, and 0.02 μ_B, respectively). We have also considered the inclusion of Zr-4d and 4s local orbitals. When these local orbitals are introduced no influence on the atomic forces was detected. The changes in the V_{ii} components of the EFG at the Ta are smaller than 0.1×10^{21} V/m^2.

Finally, and in order to check how the results depend on the lattice parameters we also performed calculations using a, b, c, and β values reported by Hann *et al.* ($a = 5.1505_4$ Å, $b = 5.2031_4$ Å, $c = 5.3154_4$ Å, and $\beta = 99.194_4$.[53] The differences obtained in the equilibrium structures and hyperfine properties are within the convergence tolerance.

V. RESULTS AND DISCUSSION

A. Pure m-ZrO_2

In order to check the reliability of the theoretical approach, it was applied first to the pure system in order to analyze how well-established experimental results are reproduced. Therefore, before proceeding with the study of the doped system, a summary of the main results obtained for the pure system will be given in this section.

In these calculations, the lattice parameters were fixed at their experimental values, but the internal coordinates were optimized by force minimization. The resulting internal atomic positions and the distances from Zr to its oxygen nearest neighbors (ONN) are listed in Table I. As can be seen, the results obtained for the internal parameters x, y, z using local density approximation (LDA), generalized gradient approximation (GGA), and PBE-sol are very similar and are in excellent agreement with the experimental results reported in the literature as well as previous calculations.[4,37,53–56] The mean distance predicted by the three exchange and correlation potentials (LDA: 2.156 Å, GGA: 2.157 Å, PBE-sol: 2.157 Å) are also in good agreement with those determined by x-ray diffraction (XRD, 2.158 Å, Refs. 37 and 53) and extended x-ray absorption fine structure experiments (EXAFS, 2.16 Å, Ref. 54).

The density of states (DOS) of m-ZrO_2 is presented in Fig. 2. The overall band structure of pure m-ZrO_2 is consistent with previous works (see, for example, Refs. 5, 15, 55, 57, and 58) and the semiconducting nature of this material was found: There is a gap between the valence and the conduction bands, but the usual problem of the LDA gap underestimation is observed. The minimum gap predicted by LDA is 3.6 eV (the LDA band gap is smaller by about 0.1 eV than those obtained using GGA and PBE-sol), in good agreement with other calculations,[15] whereas the experimental measured gap values are in the range 5.5–5.8 eV (Ref. 59) (a value of 5.0 eV was also reported[60]). Electron energy-loss spectroscopy (EELS) revealed a low energy gap of zirconia of 3.8 eV that was attributed to defect states.[55]

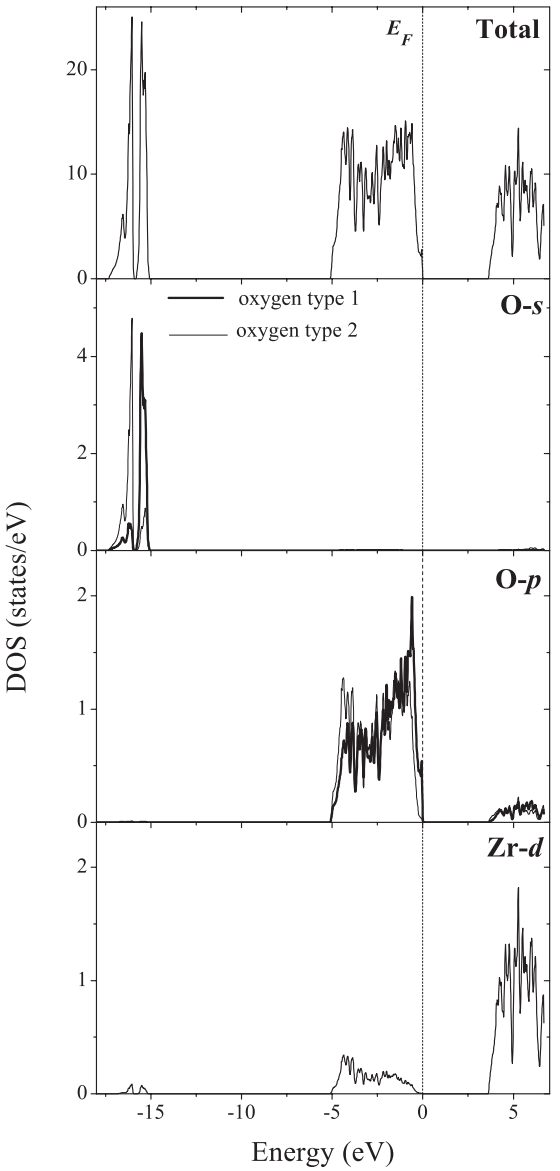

FIG. 2. Total density of states of pure m-ZrO_2 (upper panel) and Zr-d and O-p partial DOS. Energies are referred to the valence-band maximum (labeled "E_F" here) shown by a vertical dotted line.

The DOS in Fig. 2 is composed of two valence bands: a lower narrow band lying at about 15–17 eV below the valence-band maximum comprised mainly of O-2s states and an upper band between –6.0 and 0.0 eV that has mainly O-2p character with a contribution of Zr-4d character that evidence the covalent nature of the Zr-O bonds. The conduction band is composed of mainly Zr-4d with some admixture of O-2p states.

Now we will focus attention on the hyperfine properties. The major principal tensor component (V_{ZZ}) and asymmetry parameter (η) at the Zr site were calculated using both the experimental positions and the calculated, relaxed coordinates. The V_{ZZ} and η values obtained with the experimental atomic coordinates for the three exchange and correlation potentials are nearly the same within the convergence tolerance (see Table II), i.e., for a given structure the three potentials give nearly the same EFG. But when the V_{ZZ} and η are calculated for the relaxed positions, changes in the asymmetry parameter

TABLE II. Calculated and experimentally determined largest component of the diagonalized EFG tensor (V_{ZZ}) and asymmetry parameter η at Zr sites in pure m-ZrO_2. The calculations were performed using the experimental atomic positions (first row) and at the equilibrium positions predicted by LDA, GGA, and PBE-sol (second row). V_{ZZ} are in units of 10^{21} V/m^2.

	LDA		GGA		PBE-sol		Expt.	
	V_{ZZ}	η	V_{ZZ}	η	V_{ZZ}	η	V_{ZZ}	η
Experimentally determined structure	+5.5	0.25	+5.4	0.24	+5.4	0.24		
Predicted equilibrium structures	+5.5	0.02	+5.5	0.12	+5.4	0.04		
^{91}Zr NMR (Ref. 61)							5.52_5	0.2_1

value are found: A clear decrease in η going from GGA to LDA and PBE-sol is observed. This difference in the η values obtained by the approximations used for the exchange and correlation potential used here can be easily understood. In the case of the calculations using the experimentally determined internal coordinates x, y, z, the calculations were performed with the same atomic positions, and very similar η values were found in all the calculations but, in the case of the refined structures, slightly different equilibrium atomic positions were predicted. These results indicate that the different η values obtained in this case can be related (due to the extreme sensitivity of the EFG to small changes in the local structure) to different equilibrium structures, as opposed to the different descriptions of the electronic structure of the undoped system. To support this we have carried out a series of calculations. We have taken the equilibrium structure predicted by GGA and, with these positions, we performed a calculation using PBE-sol, obtaining in this case $V_{ZZ} = +5.42 \times 10^{21}$ V/m^2, $\eta = 0.11$, the same result obtained using the GGA parametrization. After that, we have taken the equilibrium structure predicted by LDA and performed GGA and PBE-sol calculations. We obtained a V_{ZZ} value of about $+5.5 \times 10^{21}$ V/m^2 and $\eta < 0.05$, the same results obtained in the LDA calculation. From these results we can conclude that, when we use the same structure LDA, GGA, and PBE-sol predict the same EFG tensor and, as a consequence, very similar electronic structures for m-ZrO_2.

The EFG can be determined with high accuracy and precision by means of hyperfine techniques. In this sense, one of the isotopes of Zr (^{91}Zr) can be used as a probe in NMR experiments and, in consequence, ^{91}Zr NMR spectroscopy is perhaps the most straightforward way to directly probe the nature of zirconium sites and learning about electronic and structural zirconium environments. However, ^{91}Zr NMR experiments in the solid state are notoriously difficult and challenging due to the low resonance frequency of ^{91}Zr and the relatively large ^{91}Zr nuclear quadrupole moment. For this reason, very few ^{91}Zr NMR studies in materials have so far been reported in the literature.[61] In the case of ^{91}Zr NMR in m-ZrO_2, the spectrum is dominated by a pure quadrupolar interaction.[61] The obtained results for V_{ZZ} and η are reported in Table II. The agreement between theory and experiment for V_{ZZ} and η is very good.

With these studies, we have demonstrated that APW + lo correctly describes electronic, structural, and hyperfine properties of pure m-ZrO_2, giving us a solid basis to start the calculations for the Ta-doped system.

B. $Zr_{31}TaO_{64}$

In order to analyze the effect of the inclusion of Ta impurities in the m-ZrO_2 host, the 96-atom SC was constructed and one of the Zr atoms was replaced by a Ta atom. In order to discuss the importance of the charge state of the impurity some preliminary calculations were performed. We calculated the self-consistent electronic structure of the 96-atom SC with all atoms in their initial unrelaxed positions in order to analyze the changes in the electronic structure of the system caused by the presence of the impurity, neglecting for the moment the problem of structural relaxations. The density of states of this system is presented in Fig. 3. Since the valence of Ta is 5+, when a Ta atom replaces a Zr^{+4} atom in the SC, there is one electron in excess. Thus, the presence of the Ta impurity induces a partially filled impurity band at the bottom of the conduction band and the resulting system is metallic, as can be seen in Fig. 3. Note that the Ta d band is described as very sharp peaks indicating that interaction between Ta atoms is quite small for this SC.

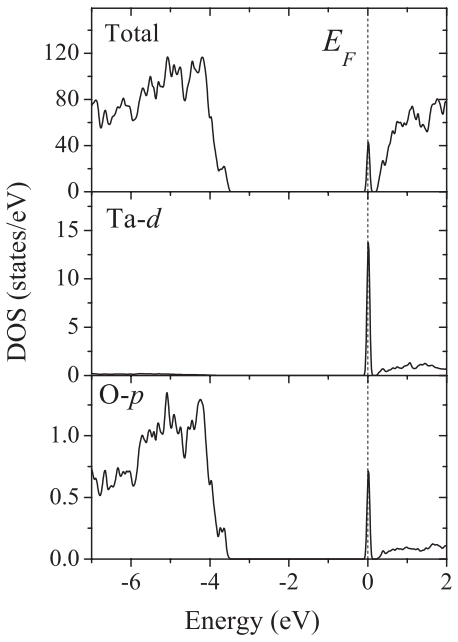

FIG. 3. Total DOS of Ta-doped m-ZrO_2 and atom-resolved PDOS of Ta (d contribution) and its ONN atoms (p contribution) for the unrelaxed system $Zr_{31}TaO_{64}$. Energies are referred to the Fermi level (E_F).

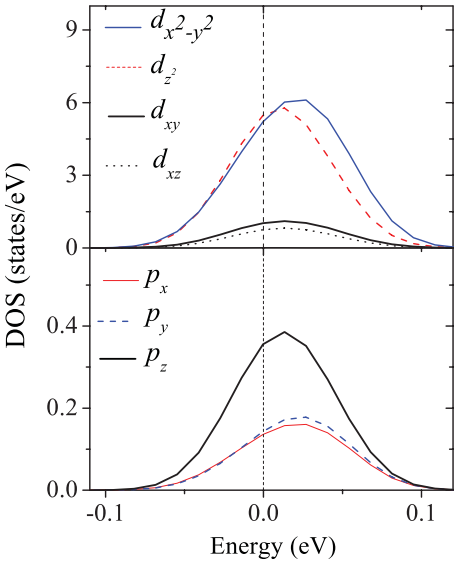

FIG. 4. (Color online) Orbital resolved partial DOS of Ta-d states and ONN-p states. The results correspond to LDA calculations for the unrelaxed system $Zr_{31}TaO_{64}$ (96-atom SC). Energies are referred to the Fermi level (E_F).

The states located at the Fermi energy (E_F) correspond to impurity states that are spatially located at Ta and at their ONN atoms and have Ta d_{z^2} and Ta $d_{x^2-y^2}$ and ONN p_x, p_y, and p_z character, as can be seen in Fig. 4. Different charge states of the impurity are related with different symmetries of the electronic charge distribution in the neighborhood of the impurity. Therefore, the charge state of the impurity can modify the structural relaxations around the impurity (due to the change of the Coulomb interaction related to the extra charge) and also strongly affect properties that depend on the fine details of the symmetry of the charge distribution in the close vicinity of the impurity.

Because the replacement of a Zr^{+4} by a Ta^{+5} can lead to, among other possibilities, two different charge states (as it was found in the similar compound m-HfO_2 (Refs. 32 and 38), we performed calculations initially considering that the impurity level remains partially filled and the extra electron introduced into the host by the Ta atom remains localized close to this atom. In the framework of an ionic model, the Ta impurity is in a $+4$ state. We will call this state the neutral charge state or $q = 0$. Secondly, we assumed that the extra electron is removed from the impurity in some way. In this case the Ta impurity is in a $+5$ state, which in this text will be called charged state or $q = +1$. In order to maintain the neutrality of the system, the extraction of the electron is compensated in our calculations by a uniform background charge distribution.

For Ta-doped m-HfO_2, APW + lo calculations have predicted (and TDPAC experiments confirmed) that, depending on the charge state of the impurity, a local magnetic moment can appear.[32] A similar result was obtained in other systems such as Cd complexes in Si and Ge.[31] Based on these results spin-polarized calculations were performed. In the case of the charged cell ($q = +1$) we did not find a magnetic solution, while in contrast, APW + lo predicts spin polarization for the case $q = 0$. For this charge state, the three XC models predict a magnetic moment of 1.00 μ_B. Total-energy calculations showed that the energy difference $\Delta E = E_{sp} - E_{nsp}$ is -0.04 eV (E_{sp} and E_{nsp} are the total energy of the spin-polarized and non-spin-polarized cases, respectively), showing that the spin-polarized cell is the energetically more stable. Similar results were obtained in the case of a larger SC.

The substitution of a Zr by a Ta atom in the m-ZrO_2 host is accompanied by a reconstruction of the positions of the surrounding atoms. In Table III we present the calculated results for the relaxed Ta-ONN bond lengths (since the results obtained using different approximations for the exchange and correlation potential are very similar, for the sake of simplicity we will present here and in the following only those obtained with GGA). It should be mentioned that for both charge states the amount of distortion per atom decreases rapidly from the oxygen nearest to the impurity to other shells. Similar to the case of m-HfO_2,[32] a contraction of the Ta-ONN bond lengths was found for both charge states. As was expected, the Ta-ONN bond lengths strongly depend on the charge state

TABLE III. Relaxed bond lengths (in Å) from the Ta impurity to its seven ONN for Ta substitutionally replacing Zr in m-ZrO_2 compared with the ones of the undoped structure. The first column is repeated from Table I for a better comparison. Calculated principal EFG component, V_{ZZ}, in units of 10^{21} V/m^2, magnetic hyperfine field, B_{HF} (in T), and asymmetry parameter η at the Ta impurity site in m-ZrO_2 are also reported.

		$q = 0$			$q = +1$		
	Unrelaxed structure	LDA	GGA	PBE-sol	LDA	GGA	PBE-sol
d(Zr-O_{1a})	2.053	2.01	2.01	2.02	1.98	1.99	1.98
d(Zr-O_{1b})	2.068	1.98	1.99	1.99	1.96	1.96	1.96
d(Zr-O_{1c})	2.150	2.06	2.08	2.07	2.08	2.06	2.08
d(Zr-O_{2a})	2.157	2.09	2.08	2.10	2.09	2.06	2.09
d(Zr-O_{2b})	2.162	2.11	2.11	2.12	2.10	2.08	2.09
d(Zr-O_{2c})	2.250	2.18	2.17	2.19	2.20	2.18	2.19
d(Zr-O_{2d})	2.251	2.19	2.19	2.19	2.21	2.18	2.20
V_{ZZ}		+18.8	+19.2	+18.7	+13.8	+13.7	+13.7
η		0.37	0.45	0.39	0.26	0.37	0.29
B_{HF}		8.7	9.2	9.0	–	–	–
μ^{SC}/μ^{Taa}		1.0/0.23	1.0/0.26	1.0/0.26	–	–	–
$\Delta E = E^{sp} - E^{nsp}$			-0.05 eV			–	

TABLE IV. Orbital populations and p and d valence contributions to the electric-field gradient at Ta substitutional sites in m-ZrO_2, in units of 10^{21} V/m^2, for the neutral ($q = 0$) and charged ($q = +1$) states of Ta in the system $Zr_{31}TaO_{64}$.

	Neutral cell ($q = 0$)			Charged cell ($q = +1$)		
	q^{up}	q^{dn}	q^{total}	q^{up}	q^{dn}	q^{total}
s	1.00	1.00	2.00	1.00	1.00	2.00
p	2.85	2.85	5.70	2.87	2.87	5.74
d	0.76	0.50	1.26	0.58	0.58	1.16
f	6.98	6.98	13.96	6.99	6.99	13.98
	Contributions to the EFG					
	Neutral cell ($q = 0$)			Charged cell ($q = +1$)		
	V_{XX}	V_{YY}	V_{ZZ}	V_{XX}	V_{YY}	V_{ZZ}
sd	+0.06	+0.18	–0.24	–0.10	–0.16	+0.26
p	–2.8	–3.6	+6.4	–6.15	–8.02	+14.17
d	–1.5	–12.0	+13.5	+0.29	+0.80	–1.09
f	–0.08	–0.19	+0.27	–0.06	–0.09	+0.15
total	–4.32	–15.61	+19.93	–6.02	–7.47	+13.49

of the impurity. In effect, as can be seen in Table III, the magnitude of the contractions is larger in the case of $q = +1$. This is due to the change caused by the extra electron in the Coulomb interactions. The contractions of the Ta-ONN bond lengths can be understood from the fact that the bond lengths in tantalum oxide (TaO_2) are about 2.02 Å.

Regarding spin polarization, we found that the magnetic moments are independent of the structural distortion, i.e., a null magnetic moment was found for $q = +1$ and a magnetic moment of 1.00 μ_B/SC for $q = 0$. In this last case, spin polarization occurs mainly at the impurity sites (0.26 μ_B/Ta; see Table IV), while the remaining moment is almost uniformly distributed over the ONN atoms and the interstitial region. Similar to the case of the unrelaxed structures, after the structural relaxations the spin-polarized solution has lower energy (for the equilibrium structures $E_{sp} - E_{nsp} = -0.05$ eV).

In the following the APW + lo results for the EFG tensor will be discussed and compared with the experimental ones. In Table III, the results for the EFG tensor (major principal component and asymmetry parameter) at the Ta site in the equilibrium structures obtained for the two charge states are given. In both cases, the differences between LDA, GGA, and PBE-sol are within the convergence tolerance. On the other hand, the difference in the EFGs obtained for the charged and neutral cells is remarkable and is not only caused by the different equilibrium structures. To understand the origin of this difference, we calculate the partial charges in the Ta muffin-tin sphere. It can be seen in Table IV that the population of the s and f states of Ta remains unaltered by the removal of one electron from the SC, while the population of the p and d orbital changes by +0.04 and –0.1 electrons from the neutral to the charged cells. Additionally, the local magnetic moment in the Ta sphere originates from the polarization of the d electrons.

In order to determine the effect of the charge difference between $q = 0$ and $q = +1$ on the EFG we focus on the valence contribution to the EFG which originates in the asymmetry of the valence charge distribution inside the muffin-tin sphere of the Ta atom. In the present case, the valence contribution is the dominant contribution and can be decomposed into the different orbital symmetries. As can be seen in Table IV the f and sd contributions to the EFG are negligible and nearly independent of the charge state of the impurity. But, the changes in the p and d populations produce drastic effects in the EFG. In the case of the neutral cell (impurity level partially occupied) the largest contribution to the EFG has it origin in the d electrons. When the impurity level is empty the d contributions drastically decrease, and the p contribution increases and becomes the dominant one. The role played by the charge state of the impurity on the symmetry of the electronic charge density can be better seen in Fig. 5. In this figure we present the atom-resolved partial density of states (PDOS) for the Ta atom in the relaxed structures of the 96-atom SC for both charge states of the impurity. As can be seen the impurity state at the Fermi level has important Ta d_{z^2} and Ta $d_{x^2-y^2}$ contributions, showing that even if small, the change in the population of the impurity state induces a drastic change in the symmetry of the charge distribution and, in consequence, of the EFG tensor.

C. Comparison with ^{181}Ta TDPAC experiments

The TDPAC technique was extensively used to characterize Zr-based systems due to the easy incorporation of the well-known ^{181}Ta probe since Hf is a natural impurity of Zr and the Ta probe is obtained from the nuclear reaction $n + {}^{180}Hf \rightarrow {}^{181}Hf + \beta^- \rightarrow {}^{181}Ta$. In these experiments, the probe is extremely diluted (ppm). Under these conditions, phase transformations and chemical reactions were investigated following the EFG behavior. In the case of m-ZrO_2, the experimental results were generally analyzed with simple models that assume that the Ta impurity probe does not produce any structural or electronic perturbation of the host and the EFG is mainly caused by the host lattice (see, for example, Refs. 62 and 63).

In the TDPAC experiments two pure nuclear quadrupole interactions (NQI) were used to describe the TDPAC spectra (see Table V). The most populated one (in the following denoted HFI1) was associated with the defect-free regular cationic sites of the monoclinic phase ($V_{zz} = 14.05_4 \times 10^{21}$ V/m^2 and $\eta = 0.335_5$; Ref. 33). The second interaction (HFI2, characterized by $V_{zz} = 21_2 \times 10^{21}$ V/m^2 and $\eta = 0.3$–0.4), was tentatively associated with Ta at cationic sites with defects.[33] Comparing the calculated EFG values of Table V and the experimental ones of Table III, it emerges that the agreement between theory and experiment is very good for both charge states, enabling us to unambiguously assign HFI1 to Ta in a regular cationic site of the monoclinic phase of m-ZrO_2 with the probe in a charged state. The other interaction also corresponds to a Ta atom in the cationic site but in this case the impurity energy level introduced by the Ta remains occupied by one electron. In other words, the Ta impurity acts as a trapping site.

Our calculations predict that, in the case of $q = 0$, the stable solution is the spin-polarized one. In consequence, HFI2 must have a combined quadrupole electric and dipolar magnetic character. Up to now, no evidence of this kind of

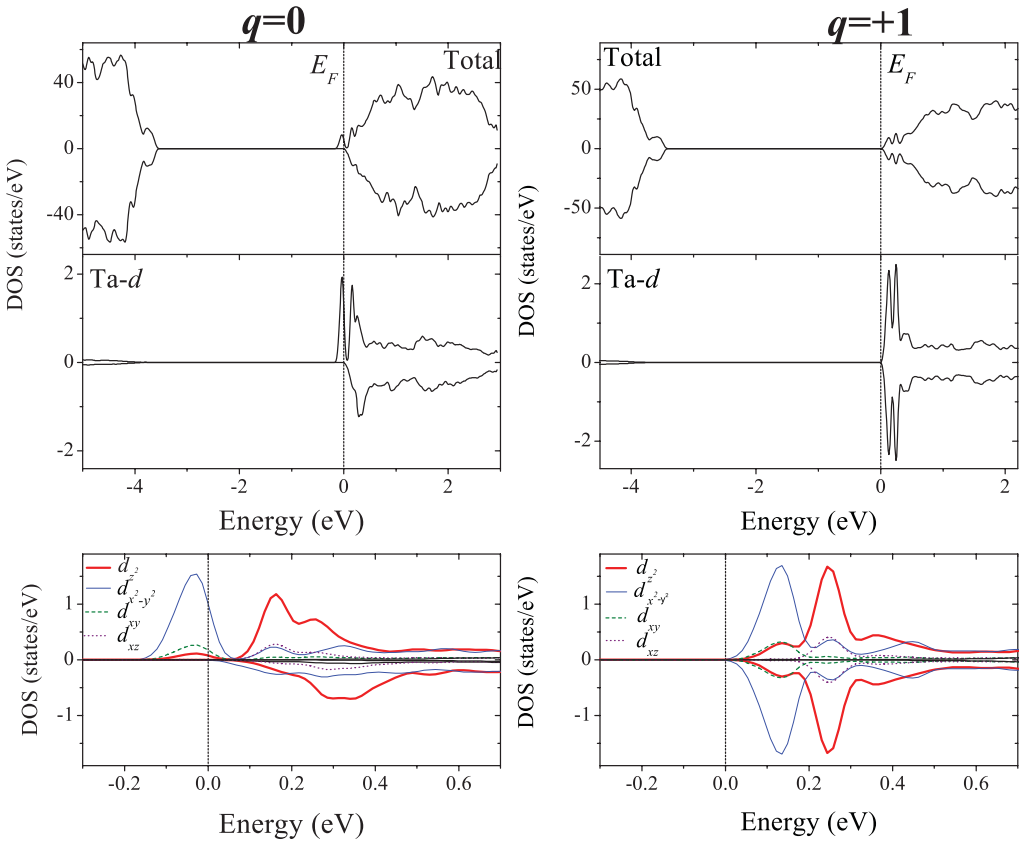

FIG. 5. (Color online) DOS of Ta-doped m-ZrO_2 (top), partial DOS of Ta d characters (middle) and orbital-resolved partial DOS of Ta d states (bottom). The results correspond to spin-polarized LDA calculations for the relaxed system $Zr_{31}TaO_{64}$ (96-atom SC) for $q = 0$ (left panels) and $q = +1$ (right panels). Energies are referred to the Fermi level (E_F). Note the change on the energy scale in the case of the orbital-resolved partial DOS of Ta d states.

combined interaction was found in the literature for Ta-doped m-ZrO_2. When the perturbation is caused by a CEMI in addition to V_{ZZ} and η, a magnetic frequency ω_L must be taken into account. Assuming that the second interaction is described by the predicted combined electric and magnetic interaction (hereafter denoted HFI2C), a new fit of the TDPAC experimental data obtained in coarse grained m-ZrO_2 (Ref. 33, with authors permission) was performed. Figure 6 shows the new fitted curve obtained by considering HFI2 as a CEMI hyperfine interaction. The obtained hyperfine parameters are summarized in Table V. The accuracy of the fit is comparable to that reported in Ref. 33. Independently of the model used for the second interaction, the fitted values corresponding to HFI1 remain unchanged. The other interaction (either HFI2 or HFI2C) represents mainly the anisotropy collapse of the TDPAC spectrum within a few nanoseconds, and in this way, it does not have enough structure to be unambiguously fitted. However, as it can be seen from Table V, HFI2 and HFI2C are characterized by very similar high V_{ZZ} values. In the case of HFI2C a value of $\omega_L = 107_1$ MHz was obtained from the fitting of the experimental TDPAC spectrum. With the use of Eq. (3) a magnetic hyperfine field $B_{HF} = 10.8$ T was derived, which is in good agreement with the calculated one ($B_{HF} = 9.2$ T). From all these results and the fact that APW + lo shows that the spin-polarized solution is energetically favorable, we conclude that the second interaction corresponds to Ta impurities located

TABLE V. Nuclear coupling constant frequency γ_Q (in MHz), electric field gradient main component V_{ZZ} (in units of 10^{21} V/m^2), asymmetry parameter η, relative frequency distribution ($\Delta\delta/\delta$), precession frequency ω_L (in MHz), and magnetic hyperfine field B_{HF} (in T) characterizing the hyperfine interactions observed in TDPAC experiments in m-ZrO_2 (Ref. 33). In order to calculate V_{ZZ} from ω_Q we used Eq. (1) and $Q(^{181}\text{Ta}) = 2.36_5$ b (Ref. 40). B_{HF} was obtained from ω_L using Eq. (3).

Model for fitting	Interaction	Relative intensity (%)	ν_Q	V_{ZZ}	η	$\Delta\delta/\delta$ (%)	ω_L	B_{hf}
Pure electric	HFI1	80	802_2	14.05_4	0.335_5	0.02_1	–	–
quadrupolar (Ref. 33)	HFI2	20	1200_{100}	21_2	0.3-0.4	0.4_{10}	–	–
CEMI	HFI1	53_2	808_2	14.16_4	0.33_1	0.03_1	–	–
(this work)	HFI2C	47_2	1200_8	21.0_1	0.46_1	0.01_1	107_1	10.8_3

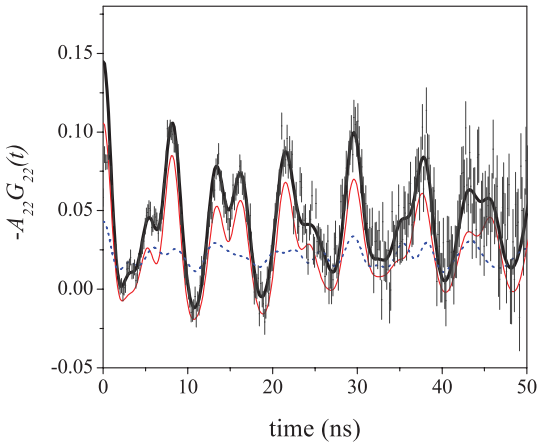

FIG. 6. (Color online) TDPAC spectrum of Ta-doped m-ZrO_2 taken at room temperature (Ref. 33) fitted with one electric quadrupolar interaction plus a CEMI. Heavy black solid line is used for the sum of HFI1 and HFI2C while thin red solid line is used for the HFI1 contribution and the dashed blue line is used for HFI2C.

at Zr sites in a neutral charge state with a net magnetic moment of about 0.26 μ_B/Ta.

VI. SUMMARY AND CONCLUSIONS

We have studied electronic, structural, and hyperfine properties of pure and Ta-doped m-ZrO_2 using state-of-the-art all-electron methods which consider atomic relaxations and the electronic structure of the doped system in a full-potential and self-consistent approach. We have also studied different charge states of the impurity and their effect on the mentioned properties. Spin-polarized solutions for each charge state were also examined.

In the case of pure m-ZrO_2 we found that the APW + lo method correctly describes the structural and electronic (apart from the "LDA gap error") properties of this semiconducting oxide. Our results for the structural properties are in excellent agreement with those obtained by XRD and EXAFS experiments. We also calculate the EFG tensor at the Zr site. Our predictions for the EFG are in excellent agreement with the experimentally determined values obtained using ^{91}Zr NMR spectroscopy. Nevertheless, the symmetry of the EFG tensor has been shown to be extremely sensitive to fine details of the atomic positions. This result suggests that a combination of accurate theoretical and experimental EFG determinations could be used as a powerful tool to probe or refine atomic positions with a high degree of accuracy.

For Ta-doped m-ZrO_2, and similar to what has previously been observed for m-HfO_2, Ta introduces impurity levels in the band gap and induces significant structural distortions (contractions of the Ta-ONN bond lengths) in the ZrO_2 host lattice. The structural distortions depend on the charge state of the impurity. For both charge states, the equilibrium Ta-ONN bond lengths are very similar to those previously found in Ta-doped m-HfO_2, showing that the local structure (at the nanoscopic scale) around Ta is nearly the same in both oxides.

Concerning hyperfine parameters, the present calculations show that the experimentally determined hyperfine interactions can be attributed to two different coexisting charge states of the Ta impurity probe atom. In the case of the $q = 0$ charge state (this charge state corresponds to the trapping of one electron by the Ta impurity), our calculations predict that the lowest energy solution corresponds to a spin-polarized state with a net magnetic moment of 1.0 μ_B/SC (0.26 μ_B in the Ta muffin-tin sphere). A new analysis of the TDPAC results supports this prediction.

The pronounced dependence of the hyperfine properties on the charge state of the impurity can be explained by analyzing the electronic structure of the defect zirconia. The difference in the EFG in magnitude and symmetry between the charged and neutral states of the impurity arises from the filling of the impurity level at the Fermi energy, mainly composed by $d_{x^2-y^2}$ levels. In consequence, the population/depopulation of this impurity level produces a drastic change in the symmetry of the charge density distribution in the close vicinity of the Ta probe atom. For this reason, the removal of one electron from the cell produces a change in the Coulomb repulsion (this is the reason for the different structural distortions predicted for each charge state) and a pronounced change in the hyperfine properties (due to the change of the symmetry of the charge distribution).

It is interesting to note that the calculated EFGs at Ta impurities substitutionally located at cationic sites in m-ZrO_2 are very similar to those previously found in Ta-doped m-HfO_2. This result (in perfect agreement with the experiments) shows that the effect of the second neighbors (Zr or Hf) on the charge distribution near Ta is negligible. To check this assertion we investigated the different contributions to the EFG, and found that the valence contribution (those originating from the nonspherical electron density of the valence and semicore electrons within the Ta muffin-tin sphere) dominates, while the lattice term is almost negligible. The valence contribution can be further decomposed according to the different orbital symmetries. In the case of $q = 0$ the main contribution comes from the d states, while in the case of $q = +1$ the EFG have essentially p character. This analysis also shows that the magnetic moment in the Ta muffin-tin sphere is predominantly due to polarization of the d electrons.

From our results it is clear that the Ta impurity heavily perturbs the m-ZrO_2 host, and that the hyperfine interactions (EFG, BHF) strongly depend on and are closely related to the electronic and structural effects induced by the impurity atom. In consequence, the impurity character of the probe and the effects that it induces in the host must be taken into account to obtain a proper description of the system.

ACKNOWLEDGMENTS

This work was partially supported by UNNOBA, Agencia Nacional de Promoción Científica y Tecnológica (ANPCyT) under Grant No. PICT98 03-03727, Consejo Nacional de Investigaciones Científicas y Técnicas (CONICET) under Grants No. PEI6174 and No. PIP6032, Fundación/Antorchas, Argentina, and the Third World Academy of Sciences

(TWAS), Italy, under Grant No. RGA 97-057. This research made use of the HP-Parallel-Computing Bose Cluster and the computational facilities at IFLP and Departamento de Física (UNLP). The authors thank M. Forker for fruitful discussion and for permitting us to use TDPAC experimental results.

*errico@fisica.unlp.edu.ar

[1] J. Čížek, O. Melikhova, I. Procházka, J. Kuriplach, R. Kužel, G. Brauer, W. Anwand, T. E. Konstantinova, and I. A. Danilenko, Phys. Rev. B **81**, 024116 (2010).

[2] A. Medevielle, F. Thévenot, and D. Tréheux, J. Eur. Ceram. Soc. **15**, 1193 (1995).

[3] *Zirconia Engineering Ceramics*, edited by E. H. Kisi (Trans Tech, Ütikon-Zürich, 1998).

[4] G. Fadda, L. Colombo, and G. Zanzotto, Phys. Rev. B **79**, 214102 (2009).

[5] J. E. Jaffe, R. A. Bachorz, and M. Gutowski, Phys. Rev. B **72**, 144107 (2005).

[6] T. Ishikawa, H. Yamaoka, Y. Harada, T. Fujii, and T. Nagasawa, Nature (London) **416**, 64 (2002).

[7] S. Meriani, *Zirconia'88. Advances in Zirconia Science and Technology* (Elsevier, New York, 1989).

[8] E. J. Walter, S. P. Lewis, and A. M. Rappe, Surf. Sci. **95**, 44 (2001).

[9] V. Fiorentini and G. Gulleri, Phys. Rev. Lett. **89**, 266101 (2002).

[10] R. O'Hayre, S.-W. Cha, W. Colella, and F. B. Prinz, *Fuel Cell Fundamentals* (Wiley, New York, 2006), Chap. 7.

[11] R. Puthenkovilakam, E. A. Carter, and J. P. Chang, Phys. Rev. B **69**, 155329 (2004).

[12] A. Meldrum, L. A. Boatner, and R. C. Ewing, Phys. Rev. Lett. **88**, 025503 (2002).

[13] C. Morant, J. M. Sanz, and L. Galán, Phys. Rev. B **45**, 1391 (1992).

[14] Ch. Jiang, X. Yang Liu, and Kurt E. Sickafus, Phys. Rev. B **83**, 052103 (2011), and references therein.

[15] H. Jiang, R. Gomez-Abal, P. Rinke, and M. Scheffler, Phys. Rev. B **81**, 085119 (2010).

[16] S. Das Sarma, Am. Sci. **89** 516 (2001).

[17] R. Janisch, P. Gopal, and N. A. Spaldin, J. Phys.: Condens. Matter **17**, R657 (2005).

[18] S. A. Chambers, Surf. Sci. Rep. **61**, 345 (2006).

[19] M. Venkatesan, C. B. Fitzgerald, J. G. Lunney, and J. M. D. Coey, Phys. Rev. Lett. **93**, 177206 (2004).

[20] J. Zippel, M. Lorenz, A. Setzer, G. Wagner, N. Sobolev, P. Esquinazi, and M. Grundmann, Phys. Rev. B **82**, 125209 (2010).

[21] S. Kuroda, N. Nishizawa, K. Takita, M. Mitome, Y. Bando, K. Osuch, and T. Dietl, Nat. Mater. **6**, 440 (2007).

[22] J. M. D. Coey, M. Venkatesan, P. Stamenov, C. B. Fitzgerald, and L. S. Dorneles, Phys. Rev. B **72**, 024450 (2005).

[23] M. Venkatesan, C. B. Fitzgerald, and J. M. D. Coey, Nature **40**, 630 (2004).

[24] J. Osorio-Guillen, S. Lany, S. V. Barabash, and A. Zunger, Phys. Rev. Lett. **96**, 107203 (2006).

[25] H. Pan, J. B. Yi, L. Shen, R. Q. Wu, J. H. Yang, J. Y. Lin, Y. P. Feng, J. Ding, L. H. Van, and J. H. Yin, Phys. Rev. Lett. **99**, 127201 (2007).

[26] D. P. Young, D. Hall, M. E. Torelli, Z. Fisk, J. L. Sarrao, J. D. Thompson, H.-R. Ott, S. B. Oseroff, R. G. Goodrich, and R. Zysler, Nature (London) **397**, 412 (1999).

[27] F. Maca, J. Kudrnovsky, V. Drchal, and G. Bouzerar, Appl. Phys. Lett. **92**, 212503 (2008).

[28] J. Osorio-Guillén, S. Lany, S. V. Barabash, and A. Zunger, Phys. Rev. B **75**, 184421 (2007).

[29] C. Das Pemmaraju and S. Sanvito, Phys. Rev. Lett. **94**, 217205 (2005).

[30] G. Bouzerar, and T. Ziman, Phys. Rev. Lett. **96**, 207602 (2006).

[31] H. Höhler, N. Atodiresei, K. Schroeder, R. Zeller, and P. H. Dederichs, Phys. Rev. B **71**, 035212 (2005); **70**, 155313 (2004).

[32] M. A. Taylor, R. E. Alonso, L. A. Errico, A. López-García, P. de la Presa, A. Svane, and N. E. Christensen, Phys. Rev. B **82**, 165203 (2010).

[33] M. Forker, P. de la Presa, W. Hoffbauer, S. Schlabach, M. Bruns, and D. V. Szabo, Phys. Rev. B **77**, 054108 (2008).

[34] A. Ayala, R. Alonso, and A. López-García, Phys. Rev. B **50**, 3547 (1994).

[35] R. J. Ackermann, S. P. Garg, and E. G. Rauh, J. Am. Ceram. Soc. **60**, 341 (1977).

[36] *Phase Equilibria Diagrams*, edited by A. E. McHale and R. S. Roth (National Institute of Standards and Technology, Gaithersburg, MD, 1996).

[37] R. C. J. Howard, R. J. Hill, and B. E. Reichert, Acta Crystallogr. B **44**, 116 (1988).

[38] R. E. Alonso, L. A. Errico, E. L. Peltzer y Blancá, A. López-García, A. Svane, and N. E. Christensen, Phys. Rev. B **78**, 165206 (2008).

[39] See, e.g., G. Schatz and A. Weidinger, *Nuclear Condensed Matter Physics—Nuclear Methods and Applications* (Wiley, Chichester, 1996); E. N. Kaufmann and R. J. Vianden, **51**, 161 (1979); H. Frauenfelder and R. M. Steffen, in *Alpha-, Beta-, and Gamma-Ray Spectroscopy*, edited by K. Siegbahn (North Holland, Amsterdam, 1966), Vol. 2.

[40] T. Butz and A. Lerf, Phys. Lett. A **97**, 217 (1983).

[41] N. J. Stone, At. Data Nucl. Data Tables **90**, 75 (2005).

[42] P. Raghavan, At. Data Nucl. Data Tables **42**, 189 (1989).

[43] M. Forker, R. Musseler, S. C. Bedi, M. Olzon-Dionysio, and S. D. de Souza, Phys. Rev. B **71**, 094404 (2005).

[44] P. de la Presa, M. Forker, J. T. Cavalcante, and A. P. Ayala, J. Magn. Magn. Mater. **306**, 292 (2006).

[45] P. Hohenberg and W. Kohn, Phys. Rev. **136**, B864 (1964); W. Kohn and L. J. Sham, *ibid.* **140**, A1133 (1965).

[46] E. Sjöstedt, L. Nordström, and D. J. Singh, Solid State Commun. **114**, 15 (2000); G. K. H. Madsen, P. Blaha, K. Schwarz, E. Sjöstedt, and L. Nordström, Phys. Rev. B **64**, 195134 (2001); See also S. Cottenier, *Density Functional Theory and the Family of (L)APW-Methods: A Step-by-Step Introduction* (KU Leuven, Belgium, 2002) [http://www.wien2k.at/reg_user/textbooks].

[47] P. Blaha, K. Schwarz, G. Madsen, D. Kvasnicka, and J. Luitz, *WIEN2k, An Augmented Plane Wave Plus Local Orbitals Program for Calculating Crystal Properties* (Karlheinz Schwarz, Technical Universität Wien, Austria, 1999).

[48]J. P. Perdew and Y. Wang, Phys. Rev. B **45**, 13244 (1992).
[49]J. P. Perdew, K. Burke, and M. Ernzerhof, Phys. Rev. Lett. **77**, 3865 (1996).
[50]J. P. Perdew, A. Ruzsinszky, G. I. Csonka, O. A. Vydrov, G. E. Scuseria, L. A. Constantin, X. Zhou1, and K. Burke, Phys. Rev. Lett. **100**, 136406 (2008).
[51]L. A. Errico, G. Fabricius, and M. Rentería, Phys. Rev. B **67**, 144104 (2003).
[52]K. Schwarz, C. Ambrosch-Draxl, and P. Blaha, Phys. Rev. B **42**, 2051 (1990).
[53]R. E. Hann, P. R. Suitchand, and J. L. Pentecost, J. Am. Ceram. Soc. **68**, C-285 (1985).
[54]P. Li, W. Cheng, and J. E. Penner-Hahn, Phys Rev B **48**, 10063 (1993).
[55]L. K. Dash, N. Vast, P. Baranek, M. Cheynet, and L. Reining, Phys. Rev. B **70**, 245116 (2004).
[56]X. Luo, W. Zhou, S. V. Ushakov, A. Navrotsky, and A. Demkov, Phys. Rev. B **80**, 134119 (2009).
[57]J. X. Zheng, G. Ceder, T. Maxisch, W. K. Chim, and W. K. Choi, Phys. Rev. B **75**, 104112 (2007).
[58]P. Dalach, D. E. Ellis, and A. van de Walle, Phys. Rev. B **82**, 144117 (2010).
[59]Experimental band gaps of ZrO_2. S. Sayan, R. A. Bartynski, X. Zhao, E. P. Gusev, D. Vanderbilt, M. Croft, M. Banaszak-Holl, and E. Garfunkel, Phys. Status Solidi B **241**, 2246 (2004); E. Bersch, S. Rangan, R. A. Bartynski, E. Garfunkel, and E. Vescovo, Phys. Rev. B **78**, 085114 (2008); R. Puthenkovilakam and J. P. Chang, Appl. Phys. Lett. **84**, 1353 (2004); S. Miyazaki, J. Vac. Sci. Technol. B **19**, 2212 (2001); H. Nohira, W. Tsai, W. Besling, E. Young, J. Petry, T. Conard, W. Vandervorst, S. De Gendt, M. Heyns, J. Maes, and M. Tuominen, J. Non-Cryst. Solids **303**, 83 (2002); R. H. French, S. J. Glass, F. S. Ohuchi, Y. N. Xu, and W. Y. Ching, Phys. Rev. B **49**, 5133 (1994); C.-K. Kwok and C. R. Aita, J. Appl. Phys. **66**, 2756 (1989).
[60]N. Ikarashi and K. Manabe, J. Appl. Phys. **94**, 480 (2003).
[61]O. B. Lapina, D. F. Khabibulin, and V. V. Terskikh, Solid State Nucl. Magn. Reson. **39**, 47 (2011).
[62]J. Luthin, K. P. Lieb, M. Neubauer, M. Uhrmacher, and B. Lindgren, Phys. Rev. B **57**, 15272 (1998).
[63]M. C. Caracoche, T. M. Dova, A. López-García, J. A. Martínez, and C. P. Rivas, Hyperfine Interact. **39**, 117 (1988).